

This manuscript has been submitted for publication in **PALEO journal**. This pre-print has **not undergone peer-review** and subsequent versions of the manuscript may differ from this version. If accepted, the final version will be available via a DOI link on this page. Please contact the corresponding author by email with any queries – [pennos4@gmail.com](mailto:pennos4@gmail.com). Prepared for EarthArxiv on 7<sup>th</sup> September 2022.

# Late Quaternary climatic histories from the Hermes Cave, Corinth Rift, Greece

*Pennos Ch.<sup>1,2</sup>, Pechlivanidou S.<sup>3</sup>, Modestou S.<sup>3,4,5</sup>, Persoiu A.<sup>2,6</sup>, Ninnemann U.<sup>3,4</sup>, Gawthorpe R.<sup>3</sup>, Maccali J.<sup>3</sup>, Lauritzen S-E.<sup>3</sup>, Skoglund R.Ø.<sup>1</sup>, Thuesen Th.<sup>3</sup>*

<sup>1</sup> Department of Geography, University of Bergen, Bergen, 5020, Norway

<sup>2</sup> Emil Racoviță Institute of Speleology, Romanian Academy, Cluj-Napoca, 400006, Romania

<sup>3</sup> Department of Earth Sciences, University of Bergen, Bergen, 5018, Norway

<sup>4</sup> Bjerknes Centre for Climate Research, Bergen, 5007, Norway

<sup>5</sup> Department of Geography and Environmental Sciences, Northumbria University, Newcastle upon Tyne, NE1 8ST, UK

<sup>6</sup> Stable Isotope Laboratory, Ștefan cel Mare University, Suceava, 720229, Romania

**Keywords:** speleothem, paleoclimate, Late Quaternary, Corinth Gulf, Eastern Mediterranean

## Abstract

The Greek peninsula is located at the crossroads of several major atmospheric circulation patterns, hence is characterized by variable climatic conditions, making it an important location to examine past climate dynamics. Over the last decades, many studies in the region focused on unravelling Holocene paleoclimatic oscillations and their impact on the development of ancient civilizations using terrestrial archives and especially speleothem records. Here, we contribute to the regional climate record over the early Holocene and late Quaternary using a speleothem from the Hermes

Cave, at the Corinth Rift shoulder in southern Greece. Our stalagmite grows over two distinct periods, from ~127 to 80 ka and from 17 to 7 ka separated by a distinct hiatus. We examine its growth history, stable isotope geochemistry and elemental composition. Higher growth rates observed during the Eemian and the early Holocene are attributed to high water recharge implying humid conditions. A gradual isotopic enrichment before the growth hiatus (~80 ka) of the stalagmite suggests a reduction in water infiltrating the system that might relate to glacier advance. Our record correlates with other paleoclimate records from the broader area confirming and extending a pattern of coherent changes in paleoclimate across the Eastern Mediterranean basin.

## **1. Introduction**

Climate in the Mediterranean Basin (MB) is a complex result of the conjunction of several atmospheric systems: westerlies from the North Atlantic Ocean, subtropical high-pressure systems originating over North Africa's arid zones, the Siberian High pressure system (SH), the North Atlantic Oscillation (NAO) (Lionello et al., 2006; Xoplaki et al., 2000) and the African and Asian Monsoons (Lionello and Galati, 2008). The NAO in particular strongly impacts winter atmospheric circulation patterns in the MB, with subsequent effects on river runoff (e.g. Tsimplis et al., 2006; Zerefos et al., 2011). Climate research continues in the MB, utilizing many different archives from the area. Many are based on marine proxies, and aim to understand the paleoceanographic evolution in the Eastern Mediterranean Basin and the prevailing paleoclimatic conditions driving that evolution (e.g. Triantaphyllou et al., 2009; Koukousioura et al., 2012; Kouli et al., 2012; Rohling et al., 2015; Triantaphyllou et al., 2015; Gogou et al., 2016; Rohling et al., 2019). Terrestrial records can also provide insight, in some cases more directly, on the paleoclimatic evolution of the area. For the wider Mediterranean area, existing records are many

and diverse, including pollen studies (e.g. Tzedakis et al., 2002; Tzedakis et al., 2006; Tzedakis, 2010; Jones et al., 2012; Milner et al., 2013), speleothems (e.g. Bar-Matthews et al., 2000; Fleitmann et al., 2009; Psomiadis et al., 2009; Finné et al., 2014; Finné et al., 2015; Nehme et al., 2015; Nehme et al., 2018; Psomiadis et al., 2018; Regattieri et al., 2018; Peckover et al., 2019; Regattieri et al., 2020), geomorphic indexes (e.g. Styllas et al., 2018; Leontaritis et al., 2020) and clastic sedimentary sequences (e.g. Lespez et al., 2017; Styllas and Ghilardi, 2017; Katrantsiotis et al., 2019; McNeill et al., 2019; Pennos et al., 2021). Despite this plethora of publications, most of the studied records do not present continuous temporal coverage for the Quaternary, and/or focus mainly on periods relevant to archaeology, when ancient civilizations flourished.

Here we aim to investigate the paleoclimatic evolution of the area from a stalagmite collected from the Corinth Rift shoulder in southern Greece which covers most of the late Quaternary and early Holocene. For these periods, this is the first published speleothem record for the Peloponnese/Gulf of Corinth region. We compare our results with other speleothem records from the broader area to understand regional scale climate dynamics, and to compliment the findings of the recent IODP Expedition 381 (McNeill et al., 2019) to decipher climate forcings affecting fluvial sediment fluxes in the Gulf of Corinth.

## **2. Setting**

Hermes cave (HC) is located on Kyllini mountain at 1614 m a.m.s.l. close to the Ziria ski resort in the Peloponnese peninsula in southern Greece (Fig.1). It is named after the ancient god Hermes, who, according to Greek mythology, was born and raised inside the cave. The cave entrance is located on a cliff facing towards Flabouritsa valley and the Gulf of Corinth. The cave has been

known since antiquity and has been visited by numerous people throughout the years who caused extensive damage to the speleothems.

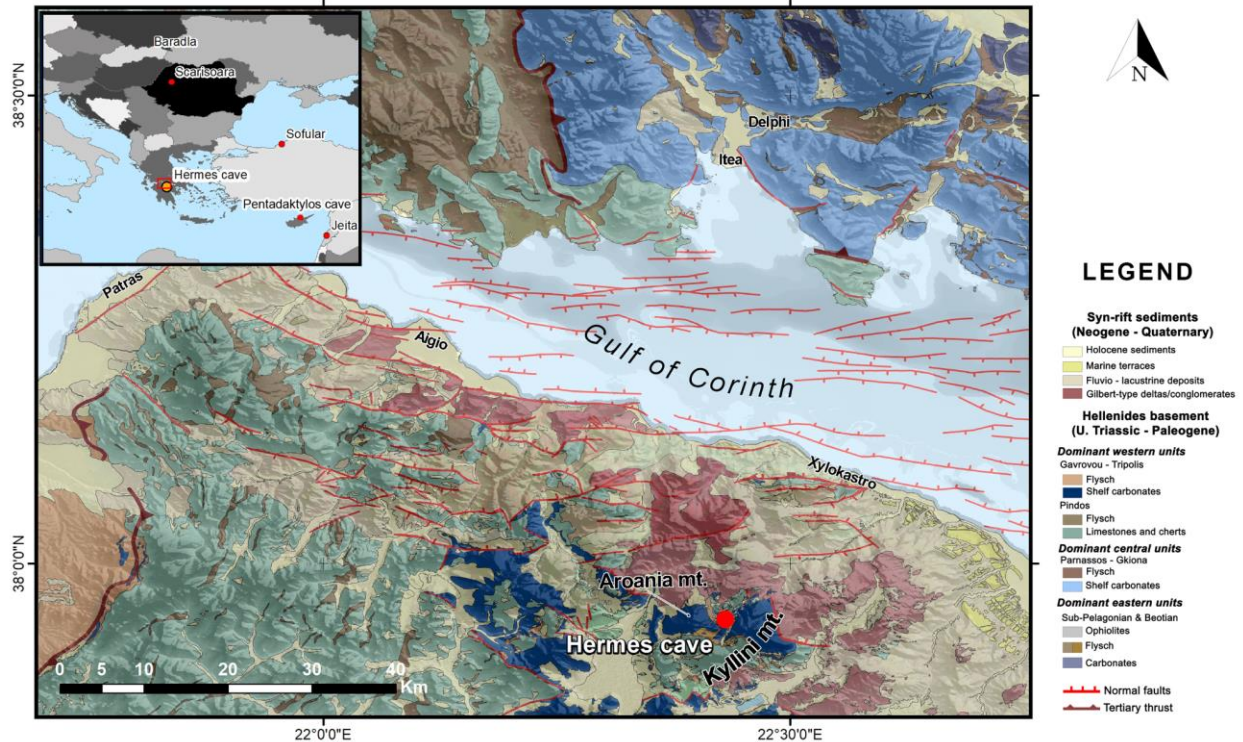


Figure 1. Regional geological map modified from Skourtsos et al. (2017). Inset shows the location of caves presented in Figs. 6 & 7.

HC formed in upper Triassic-Paleogene limestones belonging to the Gavrovo-Tripoli geotectonic zone of the Hellenides orogenic belt (e.g. Skourtsos et al., 2017; Gawthorpe et al., 2018). These carbonates outcrop on the southern flank of the Corinth extensional rift, have undergone brittle deformation and are densely fractured. The extensive fracturing has allowed surface water to penetrate into the limestone and initiate cave formation. Hermes Cave is elongated in a NE-SW direction and the cave floor dips steeply,  $> 45^\circ$ , toward the SW, following the bedding of the

limestones. Speleothem formations are extensive, with stalagmites intercepting rock debris and forming small terraces in some places.

The modern climate in the broader area corresponds to “Mediterranean Climate” with 9.7°C mean annual temperature and 1296 mm mean annual precipitation (Mamara et al., 2017). Regional climate is further characterized by mild and wet winters (December – March) that contribute most of the annual precipitation, with dry, warm summers where occasional convective precipitation occurs, resulting in strong, stormy rainfall events (Xoplaki et al., 2000; Feidas et al., 2007). Xoplaki et al. (2004) concluded that although there is large spatio-temporal variability in the region’s winter precipitation, a significant portion (30%) is explained by large-scale atmospheric circulation. This pattern is clearly observed when winter NAO-driven depressions move northeast from the North Atlantic and release rainfall on western Greece (Styllas et al., 2015 and references therein).

### **3. Methods**

#### **3.1 Speleothem sampling**

In order to collect a stalagmite that is active throughout the year, we visited the cave during the dry season (late August). We collected an active stalagmite (ZCG1) in situ from a relatively small chamber far from the entrance (Fig. 2), where no air draft was evident, to exclude drip water evaporation. The sampling chamber is a small blind passage, 6 m long, 2.5 m high and 4 m wide, that dips steeply towards the main development axis of the cave. It is located 50 m from the entrance and ~ 60 m below the surface. The ~30 cm tall stalagmite was extracted from the cave and was later cut in half along the growth axis. One part of the stalagmite was stored for reference,

and from the other half a 2 cm thick slab was extracted (see Fig. 3). From macroscopic observation it is evident that ZCG1 is a densely laminated stalagmite. Most of the banding is opaque, with no visible signs of diagenesis of the calcite fabric (Fig. 3).

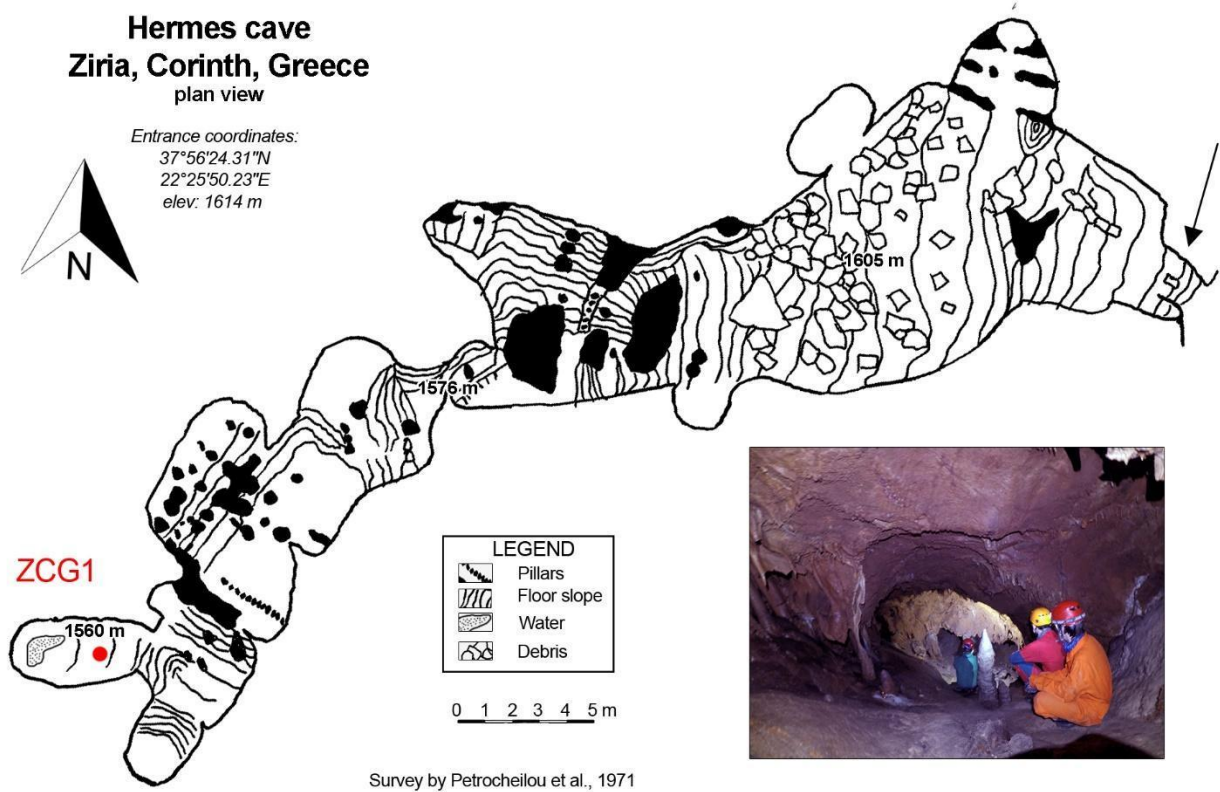


Figure 2. Plan view of Hermes Cave from Petrocheilou (1972). Red dot shows the position of the stalagmite. Inset photograph shows the chamber where stalagmite ZCG1 was formed.

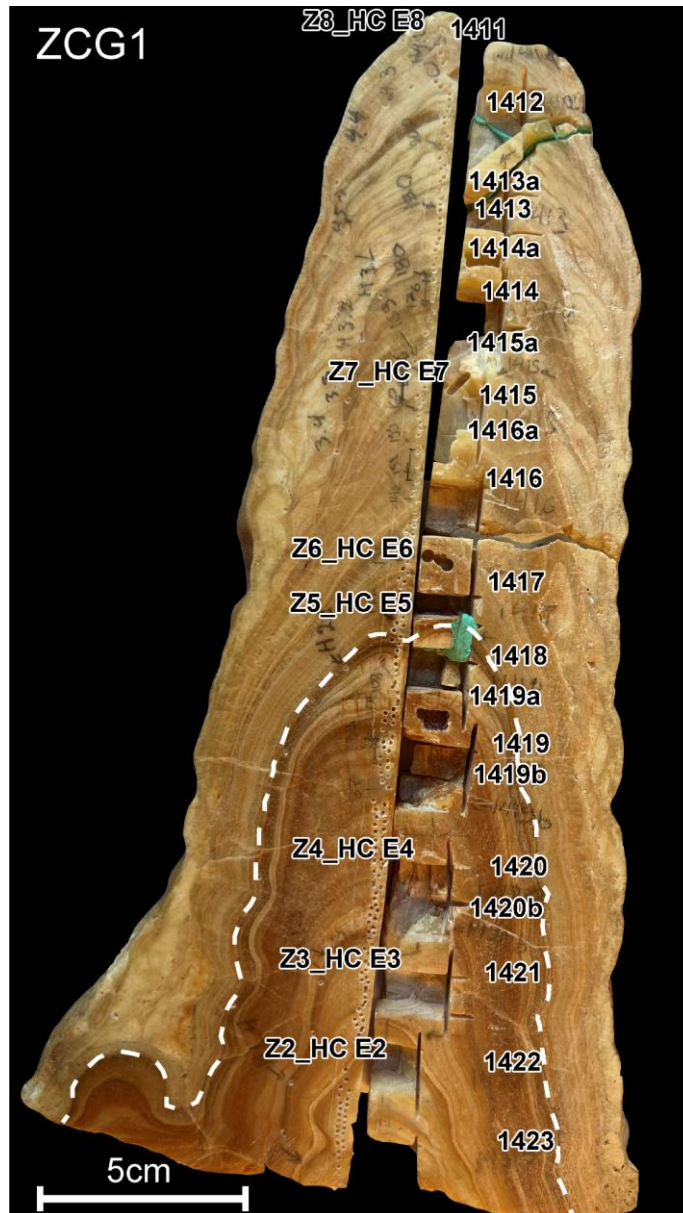


Figure 3. Polished section of the ZCG1 stalagmite. Small pits indicate stable isotope sampling position. Rectangular trenches indicate the position of the  $^{230}\text{Th}/\text{U}$  samples with their corresponding laboratory identification numbers, additional samples were extracted by hand drilling from both sides of the stalagmite slab and might not be visible (e.g. Z2\_HC E2) in this figure. White dashed line indicates the position of the growth hiatus.



### 3.2 $^{230}\text{Th}/\text{U}$ dating

To construct the age-depth model, we extracted seventeen samples along the growth axis either drilling by hand or by extracting small chunks using a rotary saw. Samples were heated at  $650^\circ\text{C}$  for 4 hours to remove organic material. Chemical separation of U and Th was adapted from Edwards (1988). The samples were spiked with a mixed  $^{233}\text{U}$ - $^{236}\text{U}$ - $^{229}\text{Th}$  solution (calibrated against Harwell Uraninite (HU-1) solution considered at secular equilibrium) and dissolved in concentrated  $\text{HNO}_3$ . Column chemistry cleaned Fe solution was added, and Fe precipitates were formed by dropwise addition of  $\text{NH}_4\text{OH}$ . Fe precipitates were rinsed with  $18.2\text{ M}\Omega$  deionized water, re-dissolved with 6 M HCl and loaded onto AG1X8 resin for U-Th separation. Uranium and Th were further purified through consecutive passes onto U/TEVA and AG1X8 resins, respectively. Th and U isotopes were analyzed on a Nu Plasma II MC-ICP-MS. Mass bias was corrected by standard-sample bracketing using HU-1 solution. Blank concentrations were  $^{238}\text{U} < 0.2\text{ ng}$ ;  $^{234}\text{U} < 30\text{ fg}$ ;  $^{232}\text{Th} < 11\text{ pg}$ ;  $^{230}\text{Th}$  was below the detection limit. Activity ratios were calculated using decay constant values from Bourdon et al. (2003). Ages were calculated using Isoplot 3.75 (Ludwig, 2003) without decay constant uncertainties. Long term analytical reproducibility of the HU-1 solution ( $n = 28$ , measured over 15 months) is  $\text{AR}(^{234}\text{U}/^{238}\text{U}) 1.002 \pm 0.001$  and  $\text{AR}(^{230}\text{Th}/^{238}\text{U}) 1.003 \pm 0.002$  (2 SD). All U-series data reported in tables are presented with  $\pm 2\sigma$  uncertainty, propagated to include analytical and spike calibration uncertainties, unless otherwise indicated.

### 3.3 Stable isotopes

Sampling for stable isotope analyses was performed by hand drilling with a 0.7 mm diameter bit along the growth axis, with 1 mm step, resulting in a total of 218 samples.  $\delta^{18}\text{O}$  and  $\delta^{13}\text{C}$  analyses were conducted at the University of Bergen (FARLAB) using a MAT 253 mass spectrometer coupled to an automated Kiel IV preparation device. Approximately 50 ( $\pm 20$ )  $\mu\text{g}$  of sample powder was reacted with concentrated ortho-phosphoric acid ( $\text{H}_3\text{PO}_4$ ) at a constant 70 °C. Isotope values are reported on the Vienna Pee Dee Belemnite (VPDB) scale calibrated using the scale reference standard NBS 19 (value 1.95‰ and 2.2‰ for  $\delta^{13}\text{C}$  and  $\delta^{18}\text{O}$ , respectively) together with NBS 18 (-5.01‰ and -23.2‰ for  $\delta^{13}\text{C}$  and  $\delta^{18}\text{O}$ , respectively; Friendman et al., 1982; Hut, 1987; Stiltcher, 1993; Coplen et al., 2006). Analytical reproducibility (1s), based on replicate measurements of the in-house carrara marble standard CM12, and spanning the same mass range and run over the same analysis period (n=128), was 0.06 and 0.03 for  $\delta^{18}\text{O}$  and  $\delta^{13}\text{C}$ , respectively. Finally, we performed Hendy's tests (Hendy, 1971) within 4 distinct bands as a first check for correlation between  $\delta^{18}\text{O}$  and  $\delta^{13}\text{C}$ , providing information about possible kinetic effects during precipitation.

### **3.4 $\mu$ -XRF**

Relative elemental composition was determined by x-ray fluorescence using an Itrax core scanner. Core scanning was conducted on the 2 cm thick stalagmite slab, along the growth axis at 1 mm intervals using a Mo x-ray tube (Croudace et al., 2006). Exposure time was 10 s, power supply was 30 kV/55 mA. The output was later processed using Q-spec software.

## **4. Results**

### **4.1 Age Model and growth rate**

The  $^{230}\text{Th}/\text{U}$  analysis produced ages ranging from  $7.1 \pm 0.1$  ka to  $127.9 \pm 52.5$  ka (Table 1). To generate a growth model we used the Mod-Age software (Hercman and Pawlak, 2012) that

employs a weighted scatterplot smoothing (LOESS) interpolation to build the chronological model. Eight <sup>230</sup>Th/U dates were indicated by the software to be outliers (see Fig. 4b) and were not used for the model. The growth period covers the period 126.4 to 7.04 ka but is interrupted by a hiatus in growth at ~ 135 mm from the base. This hiatus extends between approximately 83.2 to 16.7 ka (Fig. 4a).

Table 1. Activity ratios and age calculations from ZCG1 stalagmite. The ages are corrected with mean crust value (<sup>232</sup>Th/<sup>238</sup>U ~3.8)

Sample ID	Depth midpoints (mm)	<sup>238</sup> U ppm	±	<sup>232</sup> Th ppb	±	( <sup>230</sup> Th/ <sup>238</sup> U)	±	( <sup>234</sup> U/ <sup>238</sup> U)	±	Age uncr (ka)	±	<sup>230</sup> Th/ <sup>232</sup> Th	±	Age cr (ka)	±
Z8_HC E8	6.5	0.28089019	0.003	3.69	0.01	0.070	0.001	1.093	0.015	7.2	0.1	16.4	0.2	7.1	0.1
1411	8.5	0.2221076	0.007	2.692	0.099	0.0683	0.0338	1.0782	0.0739	7.1	4.2	17.2137	8.5211	7.0	4.2
1412	26	0.19666157	0.007	3.190	0.116	0.0727	0.0451	1.0986	0.0929	7.4	5.5	13.6932	8.4893	7.3	5.5
1413a	36	0.19688207	0.001	2.512	0.010	8.18E-02	4.82E-04	1.08E+00	6.44E-03	8.6	0.1	1.96E+01	1.15E-01	8.5	0.3
1413	51	0.19551195	0.007	4.647	0.177	0.0841	0.0352	1.1025	0.0775	8.6	4.4	10.8127	4.5253	8.4	4.4
1414a	61.5	0.21866478	0.001	2.501	0.008	8.66E-02	3.98E-04	1.11E+00	5.04E-03	8.8	0.1	2.31E+01	1.06E-01	8.7	0.3
1414	72	0.21925215	0.007	3.761	0.135	0.0789	0.0222	1.0955	0.0645	8.1	2.9	14.0644	3.9512	8.0	2.9
1415a	82.5	0.22921127	0.001	12.054	0.049	0.2021	0.0012	1.0953	0.0059	22.1	0.2	11.7471	0.0702	21.9	0.6
Z7_HC E7	91.5	0.22045181	0.001	3.86	0.01	0.085	0.001	1.115	0.006	8.6	0.1	14.8	0.1	8.5	0.1
1415	97	0.18648196	0.006	2.252	0.086	0.0795	0.0447	1.1091	0.0784	8.1	5.4	20.1112	11.3300	8.0	5.4
1416a	105	0.34383133	0.001	2.425	0.010	7.02E-02	3.96E-04	1.11E+00	6.29E-03	7.1	0.1	3.04E+01	1.72E-01	7.0	0.2
1416	119.5	0.17815697	0.006	10.242	0.409	0.1033	0.0431	1.1233	0.0940	10.5	5.6	5.4296	2.2664	10.0	5.5
Z6_HC E6	128.5	0.17501238	0.001	39.66	0.13	0.168	0.001	1.130	0.007	17.5	0.2	2.3	0.0	15.6	0.2
1417	141.5	0.16524848	0.008	46.196	1.924	0.2129	0.0688	1.1250	0.1184	22.7	11.2	2.3270	0.7511	20.4	11.0
Z5_HC E5	144.5	0.13103445	0.001	22.75	0.07	0.643	0.006	1.196	0.007	81.9	1.3	11.3	0.1	80.6	1.3
1418	156.5	0.07748967	0.008	19.259	1.481	0.7299	0.1407	1.1537	0.1831	105.6	97.0	8.9752	1.6007	103.6	96.6
1419a	168.5	0.11708911	0.000	24.839	0.100	7.04E-01	4.02E-03	1.13E+00	6.68E-03	104.1	1.5	1.01E+01	5.71E-02	102.8	5.8
1419	179.5	0.10695473	0.005	34.434	3.014	0.7381	0.1202	1.1007	0.0961	117.7	65.8	7.0064	1.2527	115.1	65.6
1419b	187	0.12610541	0.001	19.4514289	0.088	0.7063	0.0045	1.1121	0.0069	107.0	1.7	13.9950	0.0916	107.9	5.0
Z4_HC E4	196.5	0.13461639	0.001	13.77	0.04	0.650	0.006	1.145	0.010	89.3	1.8	19.4	0.1	88.5	1.8
1420b	217.5	0.1580759	0.001	46.9540097	0.19237715	0.7541	0.0043	1.1400	0.0064	114.1	1.7	7.7589	0.0452	114.1	5.4
Z3_HC E3	246.5	0.22515075	0.001	17.17	0.05	0.725	0.005	1.084	0.009	118.1	2.6	29.1	0.2	117.4	2.6
Z2_HC E2	268.5	0.18563502	0.001	5.13	0.02	0.653	0.006	1.092	0.009	97.7	1.9	72.2	0.5	97.5	1.9
1423	278.5	0.24304054	0.008	11.249	0.429	0.7381	0.0879	1.0565	0.0670	128.3	52.5	48.7381	5.8633	127.9	52.5

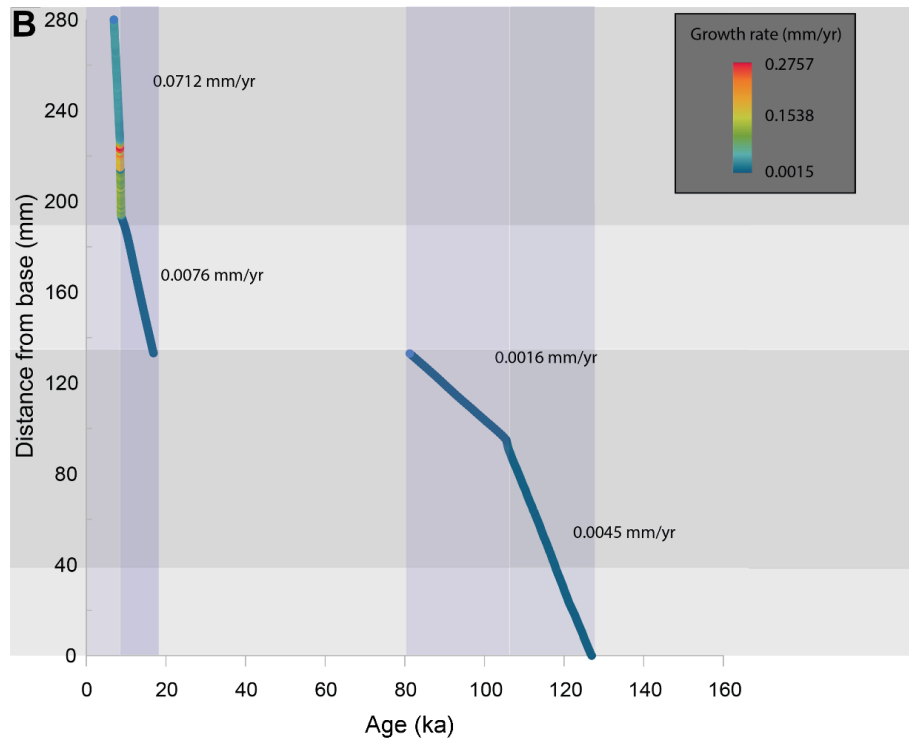
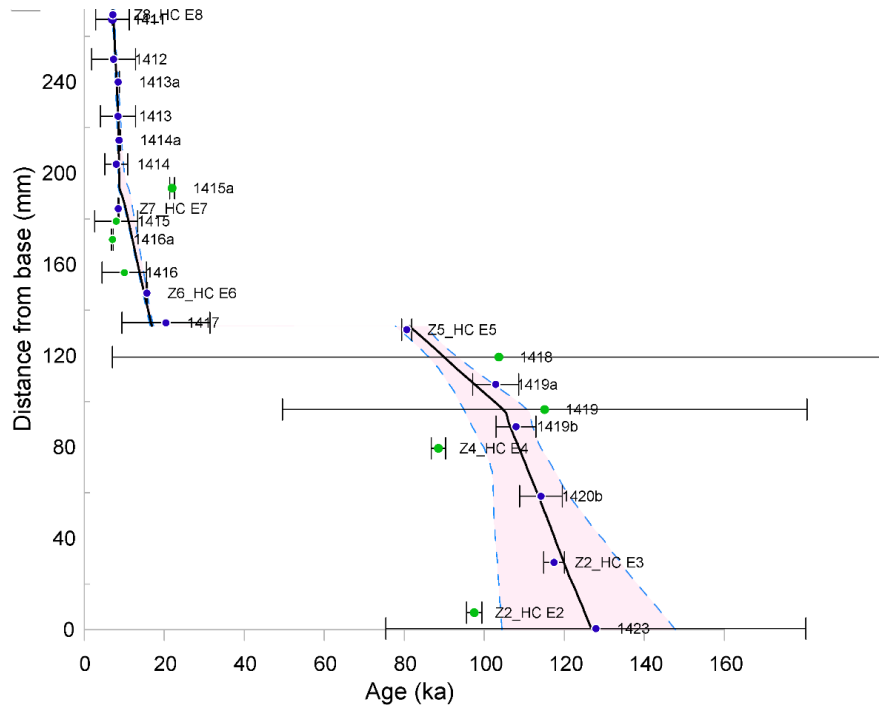


Figure 4. A) Age depth model (blue dots = dates, horizontal error bars =  $2\sigma$  uncertainty; red shading = age model  $2\sigma$  uncertainty). Outliers removed from the model shown in green. B) Mean growth rates of the stalagmite indicated per 4 major intervals.

To estimate the growth rate for each interval, we employed a linear regression approach. Four different linear regression lines with high coefficient ( $R^2 > 0.85$ ) were generated. The oldest part of the stalagmite developed between 126.9 ka to 104.9 ka at a rate of  $4.5 \times 10^{-3}$  mm/yr. In addition the part between 97 -133 mm covers the period from 104.4 ka to 81.2 ka and exhibits a growth rate of  $1.6 \times 10^{-3}$  mm/yr. Following the growth hiatus, the rate between 16.9 ka to 8.9 ka was higher at  $7.6 \times 10^{-3}$  mm/yr. Finally, the youngest part of the stalagmite, 8.8 ka to 6.9 ka, formed at a much higher growth rate of  $71.2 \times 10^{-3}$  mm/yr (Fig. 4b).

The age estimate for the oldest sample (1423, Table 1, Fig. 3) has relatively poor precision. This age estimate is critical for constraining the age of the oldest part of the record, thus the measurement was repeated with a new portion of stalagmite material. Unfortunately, the result of this repeat measurement was not an improvement over the original, likely due to detrital contamination. To compensate for the resulting age model uncertainty on ages older than  $\sim 117$  ka, we compare the stable isotope results grouped over the Last Interglacial (113 – 129 ka; Tzedakis et al., 2018) and Holocene (to  $\sim 12.5$  ka; Styllas et al., 2018) according to the median age model dates, and compare to the same data but given ages at the maximum and minimum values of the age model error envelope (see discussion).

#### **4.2 $\delta^{18}\text{O}$ and $\delta^{13}\text{C}$ record**

The results from the Hendy tests (Hendy, 1971) suggest isotopic equilibrium conditions during the majority of ZCG1 deposition (see supplement). It is evident that the variations of  $\delta^{18}\text{O}$  and  $\delta^{13}\text{C}$  show no positive correlation along each of the tested layers, and there is no enrichment in  $^{18}\text{O}$

towards the external part of the stalagmite. The exception to this is near the termination of growth before the hiatus, which is marked by an isotopic enrichment (Fig. 5) that might be indicative of kinetic effects, possibly due to a change in climatic conditions.

$\delta^{18}\text{O}$  values range from -8.8 to -6.2 ‰ (Fig. 5). For the first 4 ka of stalagmite development the values show minor variations from -7.7 to -6.7 ‰ until ca 121 ka. This period is followed by a period of lower values (down to -8.7 ‰) lasting nearly 9 ka. An increase in  $\delta^{18}\text{O}$  values follows, which peaks at 111 ka B.P (maxima -6.8 ‰). This period is trailed by a decrease of  $\delta^{18}\text{O}$  values until ca 108 ka where the values oscillate between -7.9 and -7.3 ‰ until 105 ka. From 105 ka to ~90 ka  $\delta^{18}\text{O}$  values increase again (maxima -6.2 ‰). From 92 ka until 83 ka, when the growth of the stalagmite altered,  $\delta^{18}\text{O}$  values decrease (minima -6.98 ‰).

Shortly after the LGM (at ~16.7 ka BP), stalagmite growth resumed and for the entire growth period, the  $\delta^{18}\text{O}$  record shows a slight increasing tendency, punctuated by several oscillations. Thus, the post-LGM  $\delta^{18}\text{O}$  record shows a weak decreasing trend between 16.75 ka and the onset of the Holocene, with minor fluctuations around a mean value of ~8.2 ‰. After the onset of the Holocene, the trend reverses, the  $\delta^{18}\text{O}$  values slightly increasing and peaking at 7.8 ka BP.

The  $\delta^{13}\text{C}$  values range between -10.4 to -3.5 ‰ VPDB (Fig. 5). From 126 ka to 121 ka,  $\delta^{13}\text{C}$  values show small variations from -8.5 to -7 ‰. From 121 to 117 ka, the carbon isotope record exhibits a slight decrease until -8.3‰. After a short and sharp  $^{13}\text{C}$  enrichment at 116.5 ka, a period of ca. 4 millennia with minor oscillations in  $\delta^{13}\text{C}$  values follows. During the next evolutionary stage of the stalagmite, a strong increase in  $\delta^{13}\text{C}$  to around -3.5 ‰ is observed and lasts for ~ 2 millennia. The following period begins with a sharp decrease of  $\delta^{13}\text{C}$  at ca 109 ka BP and continues with slight variations overprinted on this long term  $^{13}\text{C}$ -depletion until 99 ka. Following, until the stalagmite growth is interrupted at ca 83 ka the  $\delta^{13}\text{C}$  values fluctuate slightly around -5.8 ‰. In the post-LGM

growth period, the  $\delta^{13}\text{C}$  record presents abruptly decreasing values between 16.75 and 12 ka, and mostly constant during the Holocene. g.

### **4.3 $\mu$ -XRF**

The XRF measurements generated a detailed trace element profile of the stalagmite. The x-ray fluorescence signal in dense material such as speleothems is strong; consequently, the scan returned good counting results for numerous elements (e.g. Al, Si, P, Sr, Ti, Fe). Here we focus mainly on the Sr/Ca ratio since it can be used as a paleoclimate proxy (e.g. Kluge et al.; Fairchild and Treble, 2009; Wong et al., 2011; Fairchild and Baker, 2012). Six distinct intervals exhibit an excess in Sr compared to Ca at 123, 120-117, 114, 113, 108-106.5. and ca 105 to 104 ka (Fig. 5). After the depositional hiatus and up until 11 ka BP, Sr/Ca shows minor fluctuations. From 11 ka until ca 9.8 ka, there are two intervals where again an excess in Sr is observed (at 11 and 9.8 respectively). From 9.8 ka until the end of the record, there is a general increase in the Sr/Ca ratio with four peaks at 9.5, 8.9, 8.5 and 8.1 ka.

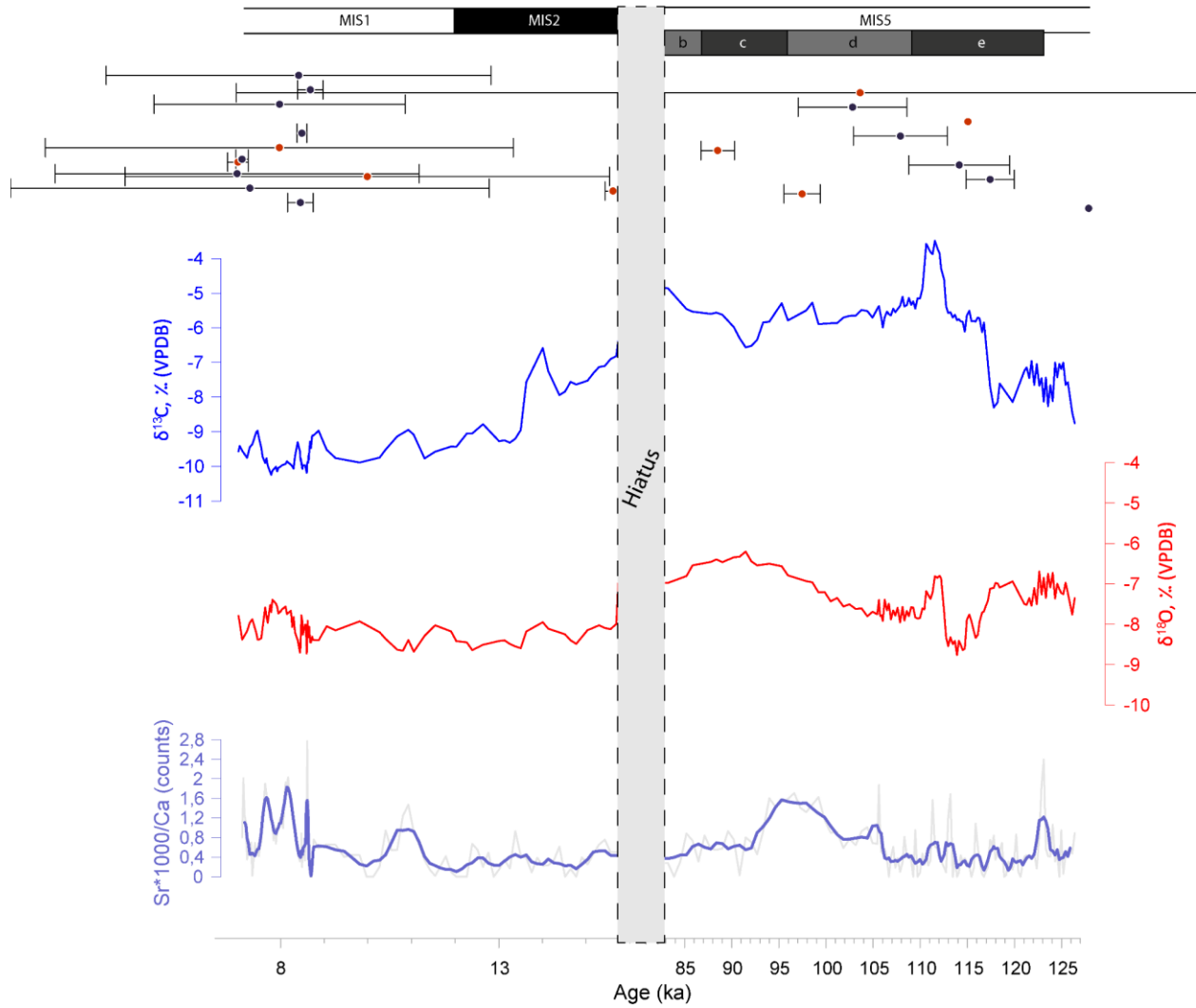


Figure 5. Carbon isotope (blue line), oxygen isotope (red line) and Sr/Ca  $\mu$ -XRF (grey and purple lines; raw data and weighted average respectively) profiles along ZCG1 stalagmite. The dating points with the  $2\sigma$  error bars are shown as black and red dots in the upper part of the figure (red dots were discarded as outliers).

## 5. Discussion

### 5.1 Major climate patterns



ZCG1 stalagmite formation initiated around 127 ka, indicating the establishment of conditions that favoured the speleothem deposition in this karstic setting. This period correlates with the beginning of the maximum interglacial conditions during MIS5 that enabled high growth rates recorded in stalagmites across Europe (Drysdale et al., 2009; Genty et al., 2013; Demeny et al., 2017). In the absence of monitoring data, we base our proxy interpretation on similar records (in terms of recharge, speleothem growth period, climatic conditions) from the wider region. We interpret the carbon isotope signal from the ZCG1 stalagmite as reflecting soil activity, which itself is dependent on both temperature and precipitation regime (e.g. Genty et al., 2001). The  $\delta^{18}\text{O}$  of calcite is more difficult to interpret in terms of both specific season it refers to and whether it is indicating climatic conditions or source  $\delta^{18}\text{O}$  (precipitation and/or moisture source). Interpretation of the ZCG1 is not simple since it can be influenced by various climate variables, such as variations in surface and cave air temperatures, seasonality of precipitation, storm tracks and ice volume (e.g. Fleitmann et al., 2009 and references within). The extent these variables controlled our record is not fully clear. However, the similarity of our record with other records in the area suggests that changes in the oxygen values reflect the combined effect of temperature and moisture source (e.g. Dansgaard, 1964; McDemott, 2004; Nehme et al., 2015 and references within) and in the absence of quantification, we only marginally discuss it in our interpretation.

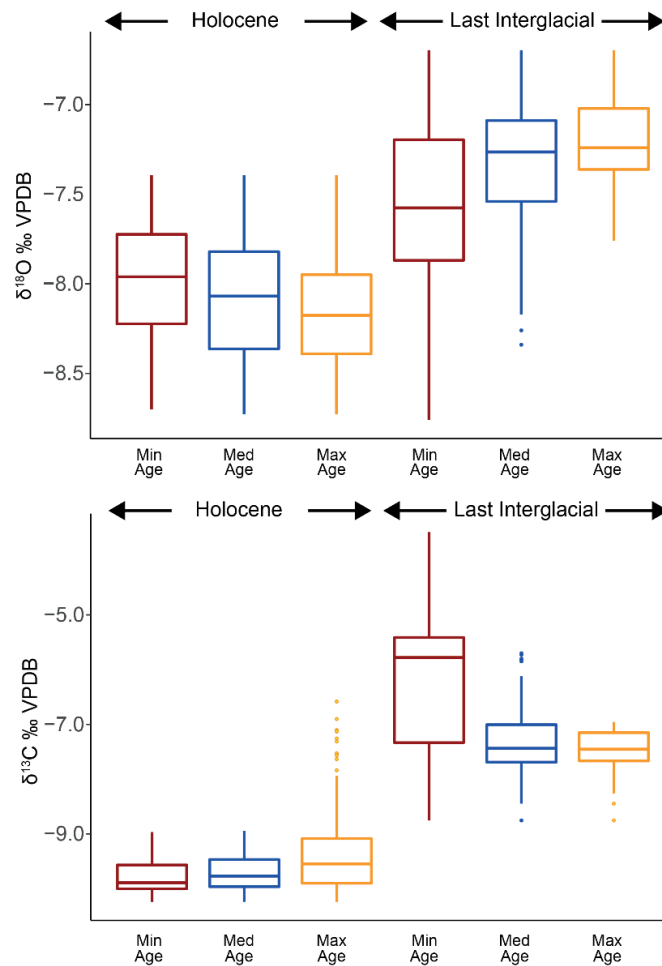


Figure 6. Box plots comparing Ziria speleothem stable isotope compositions from the Holocene (7-11.7 ka) against the Last Interglacial (127 to 116 ka) by possible ages (med age = mean age, also age model used; min age = minimum age at error envelope limit; max age = maximum age at error envelope limit).

Fig. 6 compares the stable isotope data from the Holocene (7 - 11.7 ka) with those from the Last Interglacial (116 to 127 ka), with the data grouped based on different options in the age model (mean age, minimum age according to the error envelope, maximum age according to the error envelope). As the oldest  $^{230}\text{Th}/\text{U}$  date has a large associated uncertainty, whereas it is required in

order to provide an age model to the base of the speleothem, this comparison aims to examine how the relationship between the range of isotopic compositions for each period changes with age model assignment. With the exception of  $\delta^{18}\text{O}$  compositions using minimum age values, all versions of the data are significantly different between the two time periods; each set exhibits similar differences in isotopic composition between the Holocene and Last Interglacial. This indicates that, at minimum, the different age possibilities for the oldest part of the Ziria stalagmite do not affect broad interpretations of climate for the Last Interglacial period, where the age model has the largest uncertainty. This test therefore demonstrates higher variability in stable isotope compositions, and thus likely climate, during the Last Interglacial compared to the Holocene, regardless of the selection of age model. A similar pattern has been observed in records from the North Atlantic and Southern European regions, e.g., speleothem records from Italy, marine cores and pollen records (Tzedakis et al., 2018).

#### **5.1.1. 127 - 80 ka**

Alongside the onset of initial stalagmite growth,  $\delta^{13}\text{C}$  values are increasing and  $\delta^{18}\text{O}$  values after a short decrease they increase (Fig. 7) followed by a period of instability up to 122 ka where both  $\delta^{13}\text{C}$  values and  $\delta^{18}\text{O}$  fluctuate around  $-7.5$  and  $-7$  ‰ respectively suggesting that during this part of the interglacial cycle the region had not yet reached stable interglacial conditions (Tzedakis et al., 2018). This period is also evident in both records from Baradla and Pentadaktylos caves propounding that this climatic inconsistency had a large spatial coverage, almost all over Europe. The  $\delta^{13}\text{C}$  record of ZCG1 exhibits two minima (at circa 121 and 117 ka, respectively) suggesting high soil activity that can be attributed to forest expansion due to humid conditions that is also recorded by a plethora of records (e.g., Weiberg et al., 2016). The period between these two excursions exhibits higher values, possibly corresponding to a dryer period in the region. This is

in contrast to Central European stalagmite records (e.g., Baradla cave; Demeny et al., 2017; Fig. 7) which indicates that this period is considered the optimum within the interglacial (Govin et al., 2015) with high soil activity. The  $\delta^{18}\text{O}$  record for the same period exhibits low variability, suggesting no major changes in the source or amount of precipitation; for the Gulf of Corinth this is translated in marine conditions and larger evaporation area (Gawthorpe et al., 2022). Following the  $\delta^{18}\text{O}$  values reach a minimum at ca 115 ka, while concurrently the  $\delta^{13}\text{C}$  values increase, possibly implying low soil productivity and establishment of cold and dry conditions in the area towards the onset of the MIS5d period. The same trend for both  $\delta^{13}\text{C}$  and  $\delta^{18}\text{O}$  values continues until circa 112 ka with an interruption towards 114 ka where the oxygen record exhibits a positive peak and the carbon record a negative peak. We suggest that these changes in the overall trend could be attributed to a period where cyclonic depressions forming over Africa are controlling the climate, similar to those argued to be responsible for the transport of Saharan dust to the area around this time (e.g. Stuut et al., 2009; Philandras et al., 2011; Remoundaki et al., 2011) possibly altering the source of the precipitation. The reduction in soil activity during this period is most likely related to a change in vegetation, as it corresponds chronologically to vegetation changes which occurred in the Balkan peninsula when low vegetation replaced thick interglacial forests (Tzedakis et al., 2004). This change in the type of vegetation slightly enhanced soil activity, likely resulting in the negative peak on the  $\delta^{13}\text{C}$  values at ~ 112 ka. Finally, the growth of the stalagmite continues up to ~ 80 ka until the hiatus, albeit with slightly lower  $\delta^{13}\text{C}$  values (relative to the 112 ka peak), suggesting that the area was then experiencing a period with lower soil activity. This period can be related with a change in the type of the vegetation that is transitioning to a type more resilient to arid conditions like the one described by Tzedakis (1999; Kopais record). The  $\delta^{18}\text{O}$  record during this final interval before the hiatus shows an increasing trend that peaks around 93

ka and can be attributed to higher water availability due to the establishment of interstadial conditions during MIS5c. This increase is trailed by a decrease in the  $\delta^{18}\text{O}$  values; the timing of this corresponds with the onset of MIS5b. The comparison of our record with the Pentadaktylos and Baradla cave records and the absence of clear similarities with any of the records highlights the fact that the broader area of eastern Mediterranean is in a transition zone where the climate is controlled by different systems compared to the ones controlling the climate of central Europe and eastern Mediterranean.

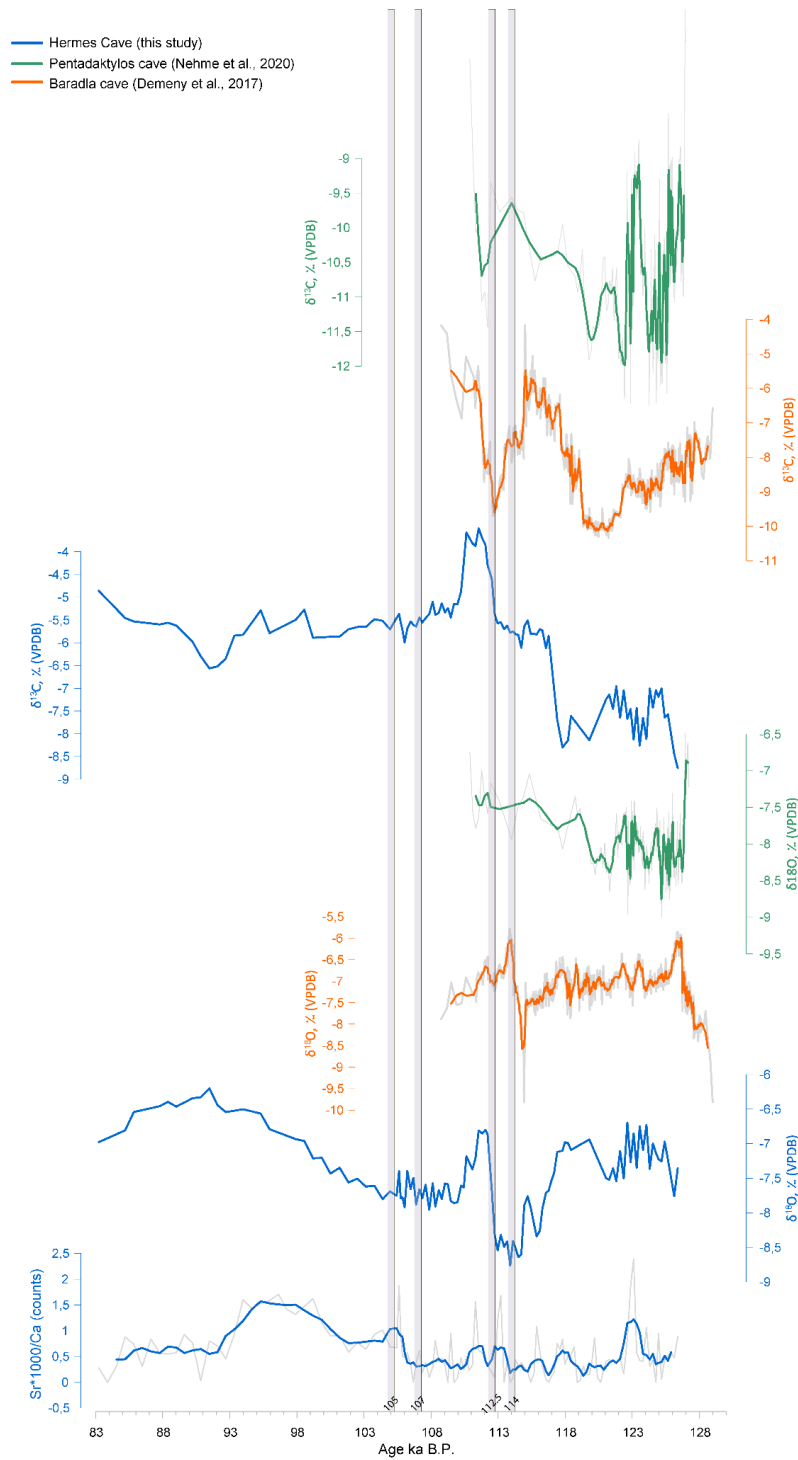


Figure 7. Comparison of ZCG1 last interglacial part with Baradla cave record (Demeny et al., 2017) and Pentadaktylos cave (Nehme et al., 2020) coloured lines for both records represent the weighted average, raw values are plotted with grey colour.

### 5.1.2. 80 - 17 ka

As warm and humid conditions are generally viewed as prerequisites for speleothem growth (Dreybrodt, 1988; Baker and Smart, 1995; Genty et al., 2006; Nehme et al., 2020), inferences about climate can potentially be made from the presence of speleothem growth hiatuses. Although the stalagmite growth hiatus might have occurred for different reasons, we suggest that in this case, the hiatus was the result of decreasing amounts of water infiltrating into the cave, possibly due to the growth of small glaciers. The ZCG1 hiatus (~ 83 to 17 ka B.P; Fig. 3) spans approximately MIS4 to the LGM; local glacier expansion during this period is evidenced in deposits on the nearby Mount Chelmos, where glacial erratics have been observed, with emplacement dated throughout MIS 3 and the LGM (Leontaritis et al., 2020). The peak of Mt. Chelmos (also known as Aroania) is of a similar elevation to Mt. Kyllini, at 2355 m and 2376 m, respectively; the peaks are essentially next to each other, with Kyllini located about 15 km east of Chelmos. Speleothem growth interruptions may also be due to a change in the fluid pathways reaching the cave and while this cannot be ruled out, the fact that ZCG1 recovered and grew throughout the Holocene makes this option less likely. MIS3 and MIS4 are thought to generally have been wetter and colder in the Eastern Mediterranean (Bar-Matthews et al., 2003, 2019), indicating conditions more suited to the development of alpine glaciers, compared to the warmer temperatures of the preceding climate phases. In particular, the Eemian (MIS5e) is estimated at 9 – 11°C warmer in the eastern Mediterranean (e.g. Nehme et al., 2020); temperatures this much higher which would have driven the snowline to a much higher altitude compared to the cooler conditions of later glacial/interglacial cycles. Cold conditions likely extended to the LGM (Styllas et al., 2015; 2018; Leontaritis et al., 2020, Hughes et al., 2022 and references within), until at the LGM termination,

when the temperature and precipitation regime no longer fulfilled the requirements for glacier preservation. After local glaciers either shrank or disappeared, water was able to once again infiltrate Hermes Cave and ZCG1 growth resumed. Similar reduced rate in speleothem growth is observed in Apuan Alps in Tuscan in Italy that is consistent with an ice coverage in the area resulting in limited availability of groundwater and the scarcity/absence of soils (Isola et al., 2019).

### **5.1.3. 17 - 7 ka**

The post-LGM part of the ZCG1 record covers the interval from 16.75 to 7 ka. Our record exhibits higher temporal resolution towards the onset of the Holocene as a result of a higher growth rate that is most likely related to the increase of precipitation amount after circa 11.7 ka cal BP.

The overall trend of  $\delta^{13}\text{C}$  record broadly follows that of similar records from regions with comparable climatic conditions, such as the Sofular Cave in Northern Turkey (Fleitmann et al., 2009) and the Jeita cave in Lebanon (Cheng et al. 2015). We have specifically chosen these records for comparison with our data as they both record winter climate variability, similar to our interpretation of  $\delta^{13}\text{C}$  and  $\delta^{18}\text{O}$  variability in the ZCG1 speleothem. While several other records exist in the area (referred to in Kern et al., 2019), these do not specifically mention what seasonally relevant climate variable is recorded so we restrict our discussion to proxies recording winter climate, only. In all these records, including the ZCG1 stalagmite,  $\delta^{13}\text{C}$  values peak at around 17 ka and drop continuously through the Late Glacial, stabilising after the onset of the Holocene. The low temporal resolution of our record during the Late Glacial does not allow us to go into detailed discussions, however, the overall similarity of these widely-spaced winter climate reconstructions suggest climatic processes acting on a regional scale. We suggest two climatic mechanisms at play during the Bolling-Allerod (BA) and Younger Dryas (YD) to be further tested by subsequent studies: 1) increased soil productivity linked to post-glacial forest expansion during the warm BA



(Feurdean et al., 2014) and 2) increased precipitation delivered by strengthened westerlies linked to the southward displacement of the polar front during the YD (Lane et al., 2013). It is conceivable that while moisture delivered along these southerly tracks reached both Greece and the Levant (as seen in the respective  $\delta^{13}\text{C}$  records), possibly also picking up moisture from the Eastern Mediterranean, they did not reach the Black Sea coast in Turkey, explaining the drier conditions observed there, as indicated by the high  $\delta^{13}\text{C}$  values during the YD in the Sofular record (Fleitmann et al., 2009). Similarly high  $\delta^{13}\text{C}$  values were recorded in speleothem P10 in SW Romania (Constantin et al., 2010) at the end of the YD, suggesting drier conditions in the northern half of the region. Collectively, these observations point towards an important differentiation of climatic conditions between SE Europe and the Eastern Mediterranean region during the YD, with a band of cold and dry climatic conditions stretching from Central Europe across the northernmost Balkan Peninsula towards the northern coast of Turkey, and somewhat wetter conditions in southern Greece and the Levant, likely brought about by moisture delivered by (the above-discussed) southward displaced westerlies. The onset of the Holocene is marked by increased variability in the  $\delta^{13}\text{C}$  and  $\delta^{18}\text{O}$  records, similar to those seen in the Jeita and Sofular records. In the Hermes Cave, several potentially cold (recorded by  $\delta^{18}\text{O}$ ) and wet (recorded by  $\delta^{13}\text{C}$ ) periods punctuate the early Holocene, broadly centred at 10.9, 8.9, 8.6, 8.4, 7.5 and 7.1 ka (Fig. 8); their timing partially correlates within error with a wet period recorded in alluvial fan formations on the Perachora peninsula (Peckover et al., 2019). These cold events that are suggested, in the absence of monitoring data, by the corresponding peaks in the nearby Jeita and Sofular records and our knowledge of modern climatic variability in the region (Xoplaki et al., 2004) are coincident with cooling events in the Carpathian Mts, as recorded by the  $\delta^{18}\text{O}$  of cave ice (Persoiu et al., 2017). These periods are further coincident within dating uncertainties with high  $\text{K}^+$  values measured in

the GISP2 record (Mayewski et al., 1997; 2004), which indicate a stronger than usual Siberian High. The Siberian High is a semi-permanent high-pressure cell located over Eurasia which affects European and Asian climate in winter (Cohen et al., 2001). Strengthening of the Siberian High results in atmospheric blocking that leads to cold air advection towards northern and central Europe and southerly outbreaks of cold air across the Aegean Sea (Rohling et al., 2002). Younger speleothem  $\delta^{18}\text{O}$  records from the Peloponnese show a contrasting response to changes in precipitation, with the Kapsia record (Finné et al., 2014) indicating high  $\delta^{18}\text{O}$  values associated with dry conditions, while the Alepotrypa record (Boyd, 2015) suggests high  $\delta^{18}\text{O}$  values are indicators of wet conditions. Under these contrasting observations, it is likely that local infiltration conditions may have an outsized effect on the  $\delta^{18}\text{O}$ -climate relationship in all studied speleothems, which would further complicate their interpretation as past climate archives.

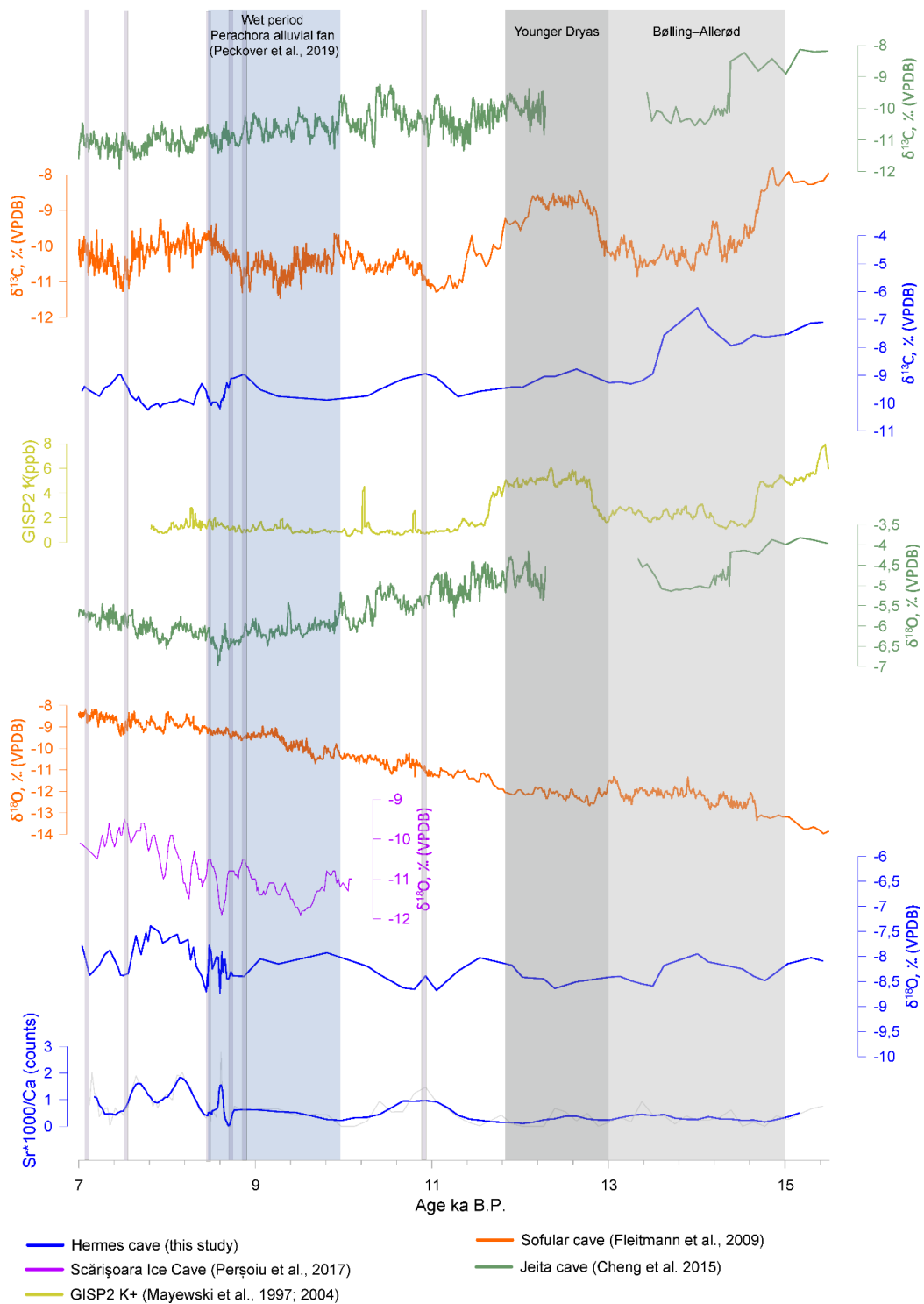


Figure 8. Comparison of ZCG1 post-LGM record with other regional records (see text for details).

#### 5.1.4. Pre and post- LGM Sr/Ca variability

$\mu$ -XRF results exhibit a relatively high variability in the Sr/Ca ratio which in combination with the stable isotope compositions can be used as indicators of seasonal environmental changes. Explaining the paleohydrologic significance of the Sr record has been proved problematic and puzzling. For the oldest part of the stalagmite the Sr/Ca ratio record shows a similar pattern to  $\delta^{18}\text{O}$ , suggesting a dependence between Sr and source/amount of precipitation within errors that comes in agreement with the work of Belli et al. (2017). Especially, for the MIS5c part of the stalagmite both proxies show an increase (Fig. 7). In detail, Sr/Ca ratio shows a prominent peak at 123-124 ka that correlates with lower values in the carbon record and high oxygen values (Fig. 7). The Sr/Ca and carbon isotope values suggest high infiltration and warm summers linked to enhanced soil production in the area, while the oxygen isotope compositions did not significantly decrease, suggesting these changes were not particularly intense. Again, an increase in local, high  $\delta^{18}\text{O}$ , moisture sources at this time would also help to explain the persisting high oxygen isotope values. The period from  $\sim$ 120 ka to 107 ka implies a period with relatively drier climatic conditions as opposed to the older part of the stalagmite. During this interval there are four prominent positive peaks at  $\sim$  117, 115, 114 and 112 ka, respectively, which broadly correlate with higher peaks in oxygen and lower peaks in the carbon record. Most probably, the area was experiencing more precipitation but the soil production was low, since there is already a transition towards the MIS5d sub-stage while mean annual temperature was decreasing. During the MIS5c sub-stage there is an increase in Sr/Ca ratio values following the observed increase in  $\delta^{18}\text{O}$  implying larger water amounts infiltrating the cave, pointing to a wetter climate until circa 96 ka when Sr values start to decrease (Fig. 7). The decrease in the Sr values doesn't follow the  $\delta^{18}\text{O}$  values suggesting that other reasons might control this change. For the post-LGM part of the stalagmite the Sr/Ca ratio

values don't present clear correlation with either the  $\delta^{18}\text{O}$  nor the  $\delta^{13}\text{C}$  and it is unclear what these changes reflect. Reggatiери et al. (2014) propose that higher trace element-to-calcium values are interpreted as responses to decreasing moisture, inducing changes in the residence time of percolation, producing prior calcite precipitation and/or variations in the hydrological routing. Based on our data we also believe that there is a temperature or precipitation threshold above/below which prior calcite precipitation occurs but due to lack of monitoring and given the resolution of the record for the post-LGM part we do not attempt any further explanation (Fig. 8).

## **5.2 Climatic impact on sediment delivery**

Recent results from the IODP Expedition 381 into the Gulf of Corinth (Shillington et al., 2019) show a profound variability in sediment accumulation rates in response to climate changes during the Quaternary. In particular, relatively low sedimentation rates (0.3 to 0.7 mm/yr) are inferred for the last interglacial period (i.e. MIS 5) in contrast to the higher sedimentation rates that characterise the last glacial (~2.5 mm/yr) and the Holocene (2.5-3 mm/yr). McNeill et al. (2019) argue that the observed variability in sediment flux is due to changes in the type of vegetation cover, while the increased sedimentation rates during the Holocene are attributed to human deforestation in the area from 6 ka onward. Our results from the lower part of the ZCG1 stalagmite suggest high soil productivity, indicative of expanded vegetation cover in the area during the oldest parts of MIS 5. During this period, erosion was likely restricted by vegetation and consequently the fluvial network delivered less sediment into the Gulf of Corinth. After the demise of peak (penultimate) interglacial conditions, over the earliest part of the ZCG1 record, our data show a decline in soil productivity inferred by higher values of  $\delta^{13}\text{C}$ . This is consistent with results from other studies that imply the development of weak vegetation cover in the Balkan peninsula (e.g. Tzedakis et al., 2004, Weiberg et al., 2016). Although stalagmite growth halts during the last glacial period

possibly due to a shortage of water infiltrating Hermes Cave as a result of the expansion of high-altitude small glaciers, at lower elevations there was probably an abundance of meltwater feeding the fluvial network. This combination of weak vegetation cover and higher water supply during the last glacial period could explain the high sedimentation rates observed in the Gulf of Corinth over this interval (McNeill et al., 2019). The younger part of the stalagmite (post growth hiatus) suggests a warmer and wetter period. However, during this period vegetation likely did not reach forest-stage as most of the soil cover was depleted due to erosion, enabling only low, open vegetation to grow (Weiberg et al., 2016). This, in combination with glacier melting, explains the higher erosion rates observed on the flanks of the Corinth Rift and increased sediment accumulation into the gulf during the onset of Holocene (McNeill et al., 2019 and references therein).

## **6. Conclusions**

This study contributes to the paleoclimatic reconstruction of the Eastern Mediterranean over the late Quaternary and early Holocene using a speleothem (ZCG1) from the Hermes Cave, which is located at the southern flanks of the Corinth Rift, central Greece. The importance of this record lies in the fact that it is the first published speleothem from the region of Northeastern Mediterranean that covers almost the entire MIS5. Our particular findings are the following:

- The ZCG1 formation started at ~127 ka marking the establishment of climatic conditions that favored the speleothem deposition. This period coincides with the beginning of the maximum interglacial conditions which enabled the high growth rates observed in stalagmites in Europe.

- We show that a low soil productivity period prevailed in the area from circa 122 ka to 117 ka implying overall dryer climatic conditions. This finding contrasts with the wetter climatic conditions observed in central Europe during the so-called ‘last Interglacial optimum’. Dry conditions settle in the area later on until the beginning of MIS4, when the stalagmite stops growing at circa 105 ka.
- The growth hiatus of ZCG1 from 83 to 17 ka occurred most probably due to low amounts of water infiltrating into the cave, likely caused by small glaciers which expanded in the area during the intervening glacial period.
- Our record exhibits higher temporal resolution towards the onset of the Holocene due to a higher growth rate. We attribute this to increased soil productivity under warmer and wetter climatic conditions.
- The ZCG1 record presents similarities with other records in the broader area of the Eastern Mediterranean. Specifically, during the Bølling-Allerød (BA) and Younger Dryas (YD) our data suggest enhanced soil productivity linked to post-glacial vegetation expansion during the warm BA and increased precipitation delivered by strengthened westerlies due to southward displacement of the polar front during the YD. Our data show a clear differentiation of climatic conditions during the YD between SE Europe and the Eastern Mediterranean region. During the Early Holocene six warm and wet periods, at ~ 10.9, 8.9, 8.6, 8.4, 7.5 and 7.1 ka, mark the overall warming trend. These warm periods may have resulted from cold air outbursts associated with a strengthened Siberian High which were nonetheless not strong enough to generate cold conditions over mainland Greece. These clockwise moving winds may also have absorbed moisture from the Aegean Sea and caused higher than usual precipitation over the area.

- Our record shows high variability in soil productivity and precipitation. The combined effect of these two parameters is the controlling factor on catchment averaged erosion rates with implications for sediment delivery into the Gulf of Corinth.

## **7. Acknowledgements**

The authors would like to express their gratitude to cavers Yorgos Sotiriadis, Charikleia Gkarlaouni, Christina Gkarlaouni and Nikolaos Kortimanitsis for their invaluable help during our visit to Hermes Cave. The Ephorate of Palaeoanthropology and Speleology of the Hellenic Ministry of Culture is thanked for granting permission to work inside the cave (ΥΠΠΟΑ/ΓΔΑΠΚ/ΕΠΣ/ΤΑΕΜΓΠ/87570/59775/1006/40). We also thank Anna Kieu-Diem Tran for assistance with the stable isotope analyses (University of Bergen). RG acknowledges the award of the VISTA Professorship from the Norwegian Academy of Science and Letters. SP and some of the analytical work was also funded by the VISTA Professorship award. AP was supported by the Romanian Ministry of Education and Research, CNCS - UEFISCDI, project number PN-III-P4-ID-PCE-2020-2723, within PNCDI III. SEL, JM and AP acknowledge the KARTSHIVES 2 project (EEA grants). This work was inspired by the conversations we had with late Prof. Patience Cowie, a great colleague and mentor.

## **8. References**

Bar-Matthews, M., Ayalon, A., and Kaufman, A. (2000). Timing and hydrological conditions of Sapropel events in the Eastern Mediterranean, as evident from speleothems, Soreq cave, Israel. *Chemical Geology* 169(1-2), 145-156. doi: 10.1016/S0009-2541(99)00232-6.



- Belli R, Borsato A, Frisia S, Drysdale R, Maas R, Greig A. (2017). Investigating the hydrological significance of stalagmite geochemistry (Mg, Sr) using Sr isotope and particulate element records across the Late Glacial-to-Holocene transition. *Geochimica et Cosmochimica Acta* 199: 247-263. doi: 10.1016/j.gca.2016.10.024
- Bourdon, B. (2003). Introduction to U-series Geochemistry. *Reviews in Mineralogy and Geochemistry* 52(1), 1-21. doi: 10.2113/0520001.
- Boyd, M. (2015). *Speleothems from Warm Climates: Holocene Records from the Caribbean and Mediterranean Regions*. Doctoral thesis, comprehensive summary, Department of Physical Geography, Stockholm University.
- Cheng, H., Sinha, A., Verheyden, S., Nader, F.H., Li, X.L., Zhang, P.Z., et al. (2015). The climate variability in northern Levant over the past 20,000 years. *Geophysical Research Letters* 42(20), 8641-8650. doi: 10.1002/2015gl065397.
- Constantin, S., Bojar, A.-V., Lauritzen, S.-E., and Lundberg, J.: Holocene and Late Pleistocene climate in the sub-Mediterranean continental environment: A speleothem record from Poleva Cave (Southern Carpathians, Romania), *Palaeogeography, Palaeoclimatology, Palaeoecology*, 243, 322–338, <https://doi.org/10.1016/j.palaeo.2006.08.001>, 2007.
- Coplen, T.B., Brand, W.A., Gehre, M., Groning, M., Meijer, H.A., Toman, B., et al. (2006). New guidelines for delta 13C measurements. *Anal Chem* 78(7), 2439-2441. doi: 10.1021/ac052027c.
- Cohen, J., Saito, K., and Entekhabi, D.: The role of the Siberian high in northern hemisphere climate variability, *Geophys. Res. Lett.*, 28, 299–302, <https://doi.org/10.1029/2000GL011927>, 2001

- Croudace, I.W., Rindby, A., and Rothwell, R.G. (2006). ITRAX: description and evaluation of a new multi-function X-ray core scanner. *Geological Society, London, Special Publications* 267(1), 51-63. doi: 10.1144/gsl.Sp.2006.267.01.04.
- Dansgaard, W. (1964). Stable isotopes in precipitation. *Tellus* 16(4), 436-468. doi: 10.1111/j.2153-3490.1964.tb00181.x.
- Demény, A., Kern, Z., Czuppon, G., Németh, A., Leél-Őssy, S., Siklósy, Z., et al. (2017). Stable isotope compositions of speleothems from the last interglacial – Spatial patterns of climate fluctuations in Europe. *Quaternary Science Reviews* 161, 68-80. doi: 10.1016/j.quascirev.2017.02.012.
- Drysdale, R.N., Hellstrom, J.C., Zanchetta, G., Fallick, A.E., Sanchez Goni, M.F., Couchoud, I., et al. (2009). Evidence for obliquity forcing of glacial Termination II. *Science* 325(5947), 1527-1531. doi: 10.1126/science.1170371.
- Fairchild, I.J., and Baker, A. (2012). *Speleothem science : from process to past environments / Ian J. Fairchild and Andy Baker ; with contributions from Asfawossen Asrat ... [et al.]*. Chichester, U.K: Wiley Blackwell.
- Fairchild, I.J., and Treble, P.C. (2009). Trace elements in speleothems as recorders of environmental change. *Quaternary Science Reviews* 28(5-6), 449-468. doi: 10.1016/j.quascirev.2008.11.007.
- Feidas, H., Noulopoulou, C., Makrogiannis, T., and Bora-Senta, E. (2007). Trend analysis of precipitation time series in Greece and their relationship with circulation using surface and satellite data: 1955-2001. *Theoretical and Applied Climatology* 87(1-4), 155-177. doi: 10.1007/s00704-006-0200-5.

- Feurdean, A., Perşoiu, A., Tanţău, I., Stevens, T., Magyari, E. K., Onac, B. P., Marković, S., Andrič, M., Connor, S., Fărcaş, S., Gałka, M., Gaudeny, T., Hoek, W., Kolaczek, P., Kuneš, P., Lamentowicz, M., Marinova, E., Michezyńska, D. J., Perşoiu, I., Płóciennik, M., Słowiński, M., Stancikaite, M., Sumegi, P., Svensson, A., Tămaş, T., Timar, A., Tonkov, S., Toth, M., Veski, S., Willis, K. J., and Zernitskaya, V. (2014). Climate variability and associated vegetation response throughout Central and Eastern Europe (CEE) between 60 and 8 ka, *Quaternary Science Reviews*, 106, 206–224, <https://doi.org/10.1016/j.quascirev.2014.06.003>, 2014.
- Finné, M., Bar-Matthews, M., Holmgren, K., Sundqvist, H.S., Liakopoulos, I., and Zhang, Q. (2014). Speleothem evidence for late Holocene climate variability and floods in Southern Greece. *Quaternary Research* 81(2), 213-227. doi: 10.1016/j.yqres.2013.12.009.
- Finné, M., Kylander, M., Boyd, M., Sundqvist, H., and Löwemark, L. (2015). Can XRF scanning of speleothems be used as a non-destructive method to identify paleoflood events in caves? *International Journal of Speleology* 44(1), 17-23. doi: 10.5038/1827-806x.44.1.2.
- Fleitmann, D., Cheng, H., Badertscher, S., Edwards, R.L., Mudelsee, M., Göktürk, O.M., et al. (2009). Timing and climatic impact of Greenland interstadials recorded in stalagmites from northern Turkey. *Geophysical Research Letters* 36(19), L19707. doi: 10.1029/2009gl040050.
- Friedman, I., O'Neil, J., and Cebula, G. (1982). Two New Carbonate Stable-Isotope Standards. *Geostandards and Geoanalytical Research* 6(1), 11-12. doi: 10.1111/j.1751-908X.1982.tb00340.x.
- Gawthorpe R.L., Fabregas N, Pechlivanidou S, Ford M, Collier R.E.L., Carter G.D.O., McNeill L.C., Shillington D.J. (2022). Late Quaternary mud-dominated, basin-floor sedimentation

- of the Gulf of Corinth, Greece: Implications for deep-water depositional processes and controls on syn-rift sedimentation. *Basin research*. doi: 10.1111/bre.12671.
- Gawthorpe, R.L., Leeder, M.R., Kranis, H., Skourtsos, E., Andrews, J.E., Henstra, G.A., et al. (2018). Tectono-sedimentary evolution of the Plio-Pleistocene Corinth rift, Greece. *Basin Research* 30(3), 448-479. doi: 10.1111/bre.12260.
- Genty, D., Baker, A., and Vokal, B. (2001). Intra- and inter-annual growth rate of modern stalagmites. *Chemical Geology* 176(1-4), 191-212. doi: 10.1016/s0009-2541(00)00399-5.
- Genty, D., Verheyden, S., and Wainer, K. (2013). Speleothem records over the last interglacial. *PAGES news* 21(1), 24-25. doi: 10.22498/pages.21.1.24.
- Gogou, A., Triantaphyllou, M., Xoplaki, E., Izdebski, A., Parinos, C., Dimiza, M., et al. (2016). Climate variability and socio-environmental changes in the northern Aegean (NE Mediterranean) during the last 1500 years. *Quaternary Science Reviews* 136, 209-228. doi: 10.1016/j.quascirev.2016.01.009.
- Govin, A., Capron, E., Tzedakis, P.C., Verheyden, S., Ghaleb, B., Hillaire-Marcel, C., et al. (2015). Sequence of events from the onset to the demise of the Last Interglacial: Evaluating strengths and limitations of chronologies used in climatic archives. *Quaternary Science Reviews* 129, 1-36. doi: 10.1016/j.quascirev.2015.09.018.
- Hendy, C.H. (1971). The isotopic geochemistry of speleothems—I. The calculation of the effects of different modes of formation on the isotopic composition of speleothems and their applicability as palaeoclimatic indicators. *Geochimica et Cosmochimica Acta* 35(8), 801-824. doi: 10.1016/0016-7037(71)90127-x.
- Hercman, H., and Pawlak, J. (2012). MOD-AGE: An age-depth model construction algorithm. *Quaternary Geochronology* 12, 1-10. doi: 10.1016/J.Quageo.2012.05.003.

- Hughes, P.D., Allard, J.L., Woodward, J.C. (2022). Glacial landscapes of the Balkans. In European Glacial Landscapes; 141-148. doi: 10.1016/b978-0-12-823498-3.00010-8
- Hut, G. (1987). "Consultants' group meeting on stable isotope reference samples for geochemical and hydrological investigations", in: *Consultants' group meeting on stable isotope reference samples for geochemical and hydrological investigations*).
- Isola I, Ribolini A, Zanchetta G, Bini M, Regattieri E, Drysdale RN, Hellstrom JC, Bajo P, Montagna P, Pons-Branchu E. (2019). Speleothem U/Th age constraints for the Last Glacial conditions in the Apuan Alps, northwestern Italy. *Palaeogeography, Palaeoclimatology, Palaeoecology* 518: 62-71. DOI: 10.1016/j.palaeo.2019.01.001
- Jones, T.D., Lawson, I.T., Reed, J.M., Wilson, G.P., Leng, M.J., Gierga, M., et al. (2012). Diatom-inferred late Pleistocene and Holocene palaeolimnological changes in the Ioannina basin, northwest Greece. *Journal of Paleolimnology* 49(2), 185-204. doi: 10.1007/s10933-012-9654-x.
- Katrantsiotis, C., Norström, E., Smittenberg, R.H., Finne, M., Weiberg, E., Hättestrand, M., et al. (2019). Climate changes in the Eastern Mediterranean over the last 5000 years and their links to the high-latitude atmospheric patterns and Asian monsoons. *Global and Planetary Change* 175, 36-51. doi: 10.1016/j.gloplacha.2019.02.001.
- Kern, Z., Demény, A., Perşoiu, A., and Hatvani, I.G. (2019). Speleothem Records from the Eastern Part of Europe and Turkey—Discussion on Stable Oxygen and Carbon Isotopes. *Quaternary* 2(3). doi: 10.3390/quat2030031.
- Kluge, T., Münster, T. S., Frank, N., Eiche, E., Mertz-Kraus, R., Scholz, D., Finné, M., and Unkel, I.: A 4000-year long Late Holocene climate record from Hermes Cave

- (Peloponnese, Greece), *Clim. Past Discuss.* [preprint], <https://doi.org/10.5194/cp-2020-47>, 2020.
- Koukousioura, O., Triantaphyllou, M.V., Dimiza, M.D., Pavlopoulos, K., Syrides, G., and Vouvalidis, K. (2012). Benthic foraminiferal evidence and paleoenvironmental evolution of Holocene coastal plains in the Aegean Sea (Greece). *Quaternary International* 261, 105-117. doi: Doi 10.1016/J.Quaint.2011.07.004.
- Kouli, K., Gogou, A., Bouloubassi, I., Triantaphyllou, M.V., Ioakim, C., Katsouras, G., et al. (2012). Late postglacial paleoenvironmental change in the northeastern Mediterranean region: Combined palynological and molecular biomarker evidence. *Quaternary International* 261, 118-127. doi: 10.1016/j.quaint.2011.10.036.
- Lane, C. S., Brauer, A., Blockley, S. P. E., and Dulski, P.: Volcanic ash reveals time-transgressive abrupt climate change during the Younger Dryas, *Geology*, 41, 1251–1254, <https://doi.org/10.1130/G34867.1>, 2013.
- Leontaritis, A.D., Kouli, K., and Pavlopoulos, K. (2020). The glacial history of Greece: a comprehensive review. *Mediterranean Geoscience Reviews*. doi: 10.1007/s42990-020-00021-w.
- Lespez, L., Glais, A., Lopez-Saez, J.-A., Le Drezen, Y., Tsirtsoni, Z., Davidson, R., et al. (2017). Middle Holocene rapid environmental changes and human adaptation in Greece. *Quaternary Research* 85(02), 227-244. doi: 10.1016/j.yqres.2016.02.002.
- Lionello, P., Malanotte-Rizzoli, P., Boscolo, R., Alpert, P., Artale, V., Li, L., et al. (2006). "The Mediterranean climate: An overview of the main characteristics and issues," in *Mediterranean*, eds. P. Lionello, P. Malanotte-Rizzoli & R. Boscolo. Elsevier), 1-26.

- Lionello, P. and Galati, M. B. (2008). Links of the significant wave height distribution in the Mediterranean Sea with the Northern Hemisphere teleconnection patterns, *Adv. Geosci.*, 17, 13–18, <https://doi.org/10.5194/adgeo-17-13-2008>.
- Ludwig, K.R. (2003). Isoplot 3.00: A geochronological toolkit for Microsoft Excel. *Berkeley Geochronology Center Special Publication* 4, 70.
- Mamara, A., Anadranistakis, M., Argiriou, A.A., Szentimrey, T., Kovacs, T., Bezes, A., et al. (2017). High resolution air temperature climatology for Greece for the period 1971-2000. *Meteorological Applications* 24(2), 191-205. doi: 10.1002/met.1617.
- Marino, G., Rohling, E.J., Sangiorgi, F., Hayes, A., Casford, J.L., Lotter, A.F., et al. (2009). Early and middle Holocene in the Aegean Sea: interplay between high and low latitude climate variability. *Quaternary Science Reviews* 28(27-28), 3246-3262. doi: 10.1016/j.quascirev.2009.08.011.
- Mayewski, P.A., Meeker, L.D., Twickler, M.S., Whitlow, S., Yang, Q., Lyons, W.B., et al. (1997). Major features and forcing of high-latitude northern hemisphere atmospheric circulation using a 110,000-year-long glaciochemical series. *Journal of Geophysical Research: Oceans* 102(C12), 26345-26366. doi: 10.1029/96jc03365.
- Mayewski, P.A., Rohling, E.E., Curt Stager, J., Karlén, W., Maasch, K.A., David Meeker, L., et al. (2004). Holocene climate variability. *Quaternary Research* 62(3), 243-255. doi: 10.1016/j.yqres.2004.07.001.
- McDermott, F. (2004). Palaeo-climate reconstruction from stable isotope variations in speleothems: a review. *Quaternary Science Reviews* 23(7-8), 901-918. doi: 10.1016/j.quascirev.2003.06.021.

- McNeill, L.C., Shillington, D.J., Carter, G.D.O., Everest, J.D., Gawthorpe, R.L., Miller, C., et al. (2019). High-resolution record reveals climate-driven environmental and sedimentary changes in an active rift. *Scientific Reports* 9(1). doi: 10.1038/s41598-019-40022-w.
- Milner, A.M., Müller, U.C., Roucoux, K.H., Collier, R.E.L., Pross, J., Kalaitzidis, S., et al. (2013). Environmental variability during the Last Interglacial: a new high-resolution pollen record from Tenaghi Philippon, Greece. *Journal of Quaternary Science* 28(2), 113-117. doi: 10.1002/jqs.2617.
- Nehme, C., Kluge, T., Verheyden, S., Nader, F., Charalambidou, I., Weissbach, T., et al. (2020). Speleothem record from Pentadactylos cave (Cyprus): new insights into climatic variations during MIS 6 and MIS 5 in the Eastern Mediterranean. *Quaternary Science Reviews* 250. doi: 10.1016/j.quascirev.2020.106663.
- Nehme, C., Verheyden, S., Breitenbach, S.F.M., Gillikin, D.P., Verheyden, A., Cheng, H., et al. (2018). Climate dynamics during the penultimate glacial period recorded in a speleothem from Kanaan Cave, Lebanon (central Levant). *Quaternary Research* 90(1), 10-25. doi: 10.1017/qua.2018.18.
- Nehme, C., Verheyden, S., Noble, S.R., Farrant, A.R., Sahy, D., Hellstrom, J., et al. (2015). Reconstruction of MIS 5 climate in the central Levant using a stalagmite from Kanaan Cave, Lebanon. *Climate of the Past* 11(12), 1785-1799. doi: 10.5194/cp-11-1785-2015.
- Peckover, E.N., Andrews, J.E., Leeder, M.R., Rowe, P.J., Marca, A., Sahy, D., et al. (2019). Coupled stalagmite – Alluvial fan response to the 8.2 ka event and early Holocene palaeoclimate change in Greece. *Palaeogeography, Palaeoclimatology, Palaeoecology*. doi: 10.1016/j.palaeo.2019.109252.



- Pennos, C., Pechlivanidou, S., Aidona, E., Bourliva, A., Lauritzen, S.-E., Scholger, R., et al. (2021). Decoding short-term climatic variations from cave sediments over the Mid-Holocene: Implications for human occupation in the Katarraktes Cave System, Northern Greece. *Zeitschrift für Geomorphologie*. doi: 10.1127/zfg/2021/0680.
- Perşoiu, A., Onac, B. P., Wynn, J. G., Blaauw, M., Ionita, M., and Hansson, M. (2017). Holocene winter climate variability in Central and Eastern Europe. *Scientific Reports* 7, 1196. doi:10.1038/s41598-017-01397-w.
- Perşoiu, A., Ionita, M., and Weiss, H. (2019). Atmospheric blocking induced by the strengthened Siberian High led to drying in west Asia during the 4.2 ka BP event – a hypothesis. *Clim. Past* 15, 781–793. doi:10.5194/cp-15-781-2019.
- Petrocheilou, A. (1972). Cave of Herme's or Cave of Pan or Cave of Apollo or Killini's hole (in Greek). *Annals of Hellenic Speleological Society* 11(5-6), 8.
- Philandras, C.M., Nastos, P.T., Kapsomenakis, J., Douvis, K.C., Tselioudis, G., and Zerefos, C.S. (2011). Long term precipitation trends and variability within the Mediterranean region. *Natural Hazards and Earth System Sciences* 11(12), 3235-3250. doi: 10.5194/nhess-11-3235-2011.
- Psomiadis, D., Dotsika, E., Albanakis, K., Ghaleb, B., and Hillaire-Marcel, C. (2018). Speleothem record of climatic changes in the northern Aegean region (Greece) from the Bronze Age to the collapse of the Roman Empire. *Palaeogeography, Palaeoclimatology, Palaeoecology* 489, 272-283. doi: 10.1016/j.palaeo.2017.10.021.
- Psomiadis, D., Dotsika, E., Zisi, N., Pennos, C., Pechlivanidou, S., Albanakis, K., et al. (2009). Geoarchaeological study of Katarraktes cave system (Macedonia, Greece): isotopic

- evidence for environmental alterations. *Geomorphologie-Relief Processus Environnement* 15(4), 229-240. doi: 10.4000/geomorphologie.7694.
- Regattieri, E., Isola, I., Zanchetta, G., Tognarelli, A., Hellstrom, J.C., Drysdale, R.N. et al. (2020). Middle - Holocene climate variability from a stalagmite from Alilica Cave (Southern Balkans). *Alpine and Mediterranean Quaternary* 1(32). doi: 10.26382/AMQ.2019.02.
- Regattieri, E., Zanchetta, G., Isola, I., Bajo, P., Boschi, C., Perchiazzi, N., et al. (2018). A MIS 9/MIS 8 speleothem record of hydrological variability from Macedonia (F.Y.R.O.M.). *Global and Planetary Change*. doi: 10.1016/j.gloplacha.2018.01.003.
- Remoundaki, E., Bourliva, A., Kokkalis, P., Mamouri, R.E., Papayannis, A., Grigoratos, T., et al. (2011). PM10 composition during an intense Saharan dust transport event over Athens (Greece). *Sci Total Environ* 409(20), 4361-4372. doi: 10.1016/j.scitotenv.2011.06.026
- Rohling, E.J., Marino, G., and Grant, K.M. (2015). Mediterranean climate and oceanography, and the periodic development of anoxic events (sapropels). *Earth-Science Reviews* 143, 62-97. doi: 10.1016/j.earscirev.2015.01.008.
- Rohling, E.J., Marino, G., Grant, K.M., Mayewski, P.A., and Weninger, B. (2019). A model for archaeologically relevant Holocene climate impacts in the Aegean-Levantine region (easternmost Mediterranean). *Quaternary Science Reviews* 208, 38-53. doi: 10.1016/j.quascirev.2019.02.009.
- Shillington, D., McNeill, L., Carter, G., and the Expedition 381 Participants. (2019). Expedition 381 Preliminary Report: Corinth Active Rift Development. *International Ocean Discovery Program*. doi: <https://doi.org/10.14379/iodp.pr.381.2019>.

- Skourtsos, E., Kranis, H., Zambetakis-Lekkas, A., Gawthorpe, R., and Leeder, M. (2017). Alpine Basement Outcrops at Northern Peloponnesus: Implications for the Early Stages in the Evolution of the Corinth Rift. *Bulletin of the Geological Society of Greece* 50(1). doi: 10.12681/bgsg.11714.
- Stichler, W. (1995). "Interlaboratory comparison of new materials for carbon and oxygen isotope ratio measurements". (International Atomic Energy Agency (IAEA)).
- Stuut, J.-B., Smalley, I., and O'Hara-Dhand, K. (2009). Aeolian dust in Europe: African sources and European deposits. *Quaternary International* 198(1-2), 234-245. doi: 10.1016/j.quaint.2008.10.007.
- Styllas, M.N., and Ghilardi, M. (2017). Early- to mid-Holocene paleohydrology in northeast Mediterranean: The detrital record of Aliakmon River in Loudias Lake, Greece. *The Holocene* 27(10), 1487-1498. doi: 10.1177/0959683617693905.
- Styllas, M.N., Schimmelpfennig, I., Benedetti, L., Ghilardi, M., Aumaître, G., Bourlès, D., et al. (2018). Late-glacial and Holocene history of the northeast Mediterranean mountains - New insights from in situ -produced  $^{36}\text{Cl}$  - based cosmic ray exposure dating of paleo-glacier deposits on Mount Olympus, Greece. *Quaternary Science Reviews* 193, 244-265. doi: 10.1016/j.quascirev.2018.06.020.
- Styllas, M.N., Schimmelpfennig, I., Ghilardi, M., and Benedetti, L. (2015). Geomorphologic and paleoclimatic evidence of Holocene glaciation on Mount Olympus, Greece. *The Holocene*. doi: 10.1177/0959683615618259
- Triantaphyllou, M.V., Gogou, A., Dimiza, M.D., Kostopoulou, S., Parinos, C., Roussakis, G., et al. (2015). Holocene Climatic Optimum centennial-scale paleoceanography in the NE

- Aegean (Mediterranean Sea). *Geo-Marine Letters* 36(1), 51-66. doi: 10.1007/s00367-015-0426-2.
- Triantaphyllou, M.V., Ziveri, P., Gogou, A., Marino, G., Lykousis, V., Bouloubassi, I., et al. (2009). Late Glacial–Holocene climate variability at the south-eastern margin of the Aegean Sea. *Marine Geology* 266(1-4), 182-197. doi: 10.1016/j.margeo.2009.08.005.
- Tsimplis MN, Zervakis V, Josey SA, Peneva EL, Struglia MV, Stanev EV, Theocharis A, Lionello P, Malanotte-Rizzoli P, Artale V, Tragou E, Oguz T. (2006). Chapter 4 Changes in the oceanography of the Mediterranean Sea and their link to climate variability. In *Mediterranean*; 227-282.
- Tzedakis P.C. (1999). The last climatic cycle at Kopais, central Greece. *Journal of the Geological Society* 156: 425-434. doi: 10.1144/gsjgs.156.2.0425
- Tzedakis, P.C. (2010). The MIS 11-MIS 1 analogy, southern European vegetation, atmospheric methane and the 'early anthropogenic hypothesis'. *Climate of the Past* 6(2), 131-144. doi: 10.5194/cp-6-131-2010.
- Tzedakis, P.C., Drysdale, R.N., Margari, V., Skinner, L.C., Menviel, L., Rhodes, R.H., et al. (2018). Enhanced climate instability in the North Atlantic and southern Europe during the Last Interglacial. *Nat Commun* 9(1), 4235. doi: 10.1038/s41467-018-06683-3.
- Tzedakis, P.C., Frogley, M.R., and Heaton, T.H.E. (2002). Duration of Last Interglacial Conditions in Northwestern Greece. *Quaternary Research* 58(1), 53-55. doi: 10.1006/qres.2002.2328.
- Tzedakis, P.C., Frogley, M.R., Lawson, I.T., Preece, R.C., Cacho, I., and de Abreu, L. (2004). Ecological thresholds and patterns of millennial-scale climate variability: The response of

- vegetation in Greece during the last glacial period. *Geology* 32(2), 109-112. doi: 10.1130/G20118.1.
- Tzedakis, P.C., Hooghiemstra, H., and Pälike, H. (2006). The last 1.35 million years at Tenaghi Philippon: revised chronostratigraphy and long-term vegetation trends. *Quaternary Science Reviews* 25(23-24), 3416-3430. doi: 10.1016/j.quascirev.2006.09.002.
- Weiberg, E., Unkel, I., Kouli, K., Holmgren, K., Avramidis, P., Bonnier, A., et al. (2016). The socio-environmental history of the Peloponnese during the Holocene: Towards an integrated understanding of the past. *Quaternary Science Reviews* 136, 40-65. doi: 10.1016/j.quascirev.2015.10.042.
- Xoplaki, E., Gonzalez-Rouco, J.F., Luterbacher, J., and Wanner, H. (2004). Wet season Mediterranean precipitation variability: influence of large-scale dynamics and trends. *Climate Dynamics* 23(1), 63-78. doi: 10.1007/s00382-004-0422-0.
- Xoplaki, E., Luterbacher, J., Burkard, R., Patrikas, I., and Maheras, P. (2000). Connection between the large-scale 500 hPa geopotential height fields and precipitation over Greece during wintertime. *Climate Research* 14(2), 129-146. doi: DOI 10.3354/cr014129.
- Zerefos, C., Repapis, C., Giannakopoulos, C., Kapsomenakis, J., Papanikolaou, D., Papanikolaou, M., et al. (2011). The climate of the Eastern Mediterranean and Greece: past, present and future. *The Environmental, Economic and Social Impacts of Climate Change in Greece*, 50-58.